Orig Life Evol Biosph (2013) 43:221–245
DOI 10.1007/s11084-013-9339-0

PREBIOTIC CHEMISTRY

Hydrogen Cyanide Production due to Mid-Size Impacts in a Redox-Neutral N_2-Rich Atmosphere

Kosuke Kurosawa · Seiji Sugita · Ko Ishibashi · Sunao Hasegawa · Yasuhito Sekine · Nanako O. Ogawa · Toshihiko Kadono · Sohsuke Ohno · Naohiko Ohkouchi · Yoichi Nagaoka · Takafumi Matsui

Received: 22 August 2012 / Accepted: 16 June 2013 /
Published online: 23 July 2013

Abstract Cyanide compounds are amongst the most important molecules of the origin of life. Here, we demonstrate the importance of mid-size (0.1–1 km in diameter) hence frequent meteoritic impacts to the cyanide inventory on the early Earth. Subsequent aerodynamic ablation and chemical reactions with the ambient atmosphere after oblique impacts were investigated by both impact and laser experiments. A polycarbonate projectile and graphite were used as laboratory analogs of meteoritic

K. Kurosawa · K. Ishibashi · S. Ohno · Y. Nagaoka · T. Matsui
Planetary Exploration Research Center, Chiba Institute of Technology, 2-17-1, Tsudanuma, Narashino, Chiba 275-0016, Japan

K. Ishibashi
e-mail: ko.ishibashi@perc.it-chiba.ac.jp

S. Ohno
e-mail: ohno@perc.it-chiba.ac.jp

Y. Nagaoka
e-mail: yoichi.nagaoka@perc.it-chiba.ac.jp

T. Matsui
e-mail: matsui@perc.it-chiba.ac.jp

S. Sugita · Y. Sekine
Department of Complexity Science and Engineering, The University of Tokyo, 5-1-5, Kashiwanoha, Kashiwa, Chiba 277-8561, Japan

S. Sugita
e-mail: sugita@k.u-tokyo.ac.jp

Y. Sekine
e-mail: sekine@k.u-tokyo.ac.jp

S. Hasegawa
Institute of Space and Astronautical Science, Japan Aerospace Exploration Agency, 3-1-1, Yoshinodai, Chuo-ku, Sagamihara, Kanagawa 252-5210, Japan
e-mail: hasehase@isas.jaxa.jp

organic matter. Spectroscopic observations of impact-generated ablation vapors show that laser irradiation to graphite within an N_2-rich gas can produce a thermodynamic environment similar to that produced by oblique impacts. Thus, laser ablation was used to investigate the final chemical products after this aerodynamic process. We found that a significant fraction (>0.1 mol%) of the vaporized carbon is converted to HCN and cyanide condensates, even when the ambient gas contains as much as a few hundred mbar of CO_2. As such, the column density of cyanides after carbon-rich meteoritic impacts with diameters of 600 m would reach ~10 mol/m^2 over ~10^2 km^2 under early Earth conditions. Such a temporally and spatially concentrated supply of cyanides may have played an important role in the origin of life.

Keywords Hydrogen cyanide · Redox-neutral atmosphere · Hypervelocity impacts · Aerodynamic ablation · Mass spectrometry · Emission spectroscopy

Introduction

The geologic record on the Moon investigated by the Apollo Project showed that the impact flux on Earth at >3.8 Ga during the heavy bombardment period was at least ~10^3 times more than that on the present Earth (e.g., BVSP 1981; Ryder 1990; Chyba 1991). During the heavy bombardment period, the influx of both material and energy into the Earth may have been the largest during its history. Such intense bombardment may have controlled the evolution of surface environments on the early Earth. Geologic evidence suggests that the emergence of life occurred ~3.8 Ga (Schidlowski 1988; Rosing 1999), at the termination of the heavy bombardment period.

Cyanides are considered as being amongst the most important and necessary compounds in the chemical evolution phase of the origin of life (e.g., Ferris and Hagan 1984). For example, concentrated solutions of HCN (0.1–0.01 mol/L) can produce nucleic acid bases (e.g., Chang et al. 1983; Ferris and Hagan 1984; Miyakawa et al. 2002a, b). Moreover, mixtures of HCN, NH_3, aldehyde compounds, and nitrile compounds can produce amino acids (e.g., Chang et al. 1983; Ferris and Hagan 1984; Miyakawa et al. 2002a, b). Thus, a number of cyanide production processes on the early Earth have been proposed, including lightning (e.g., Miller 1953; Chameides and Walker 1981; Miller and Schlesinger 1983;

N. O. Ogawa · N. Ohkouchi
Institute of Biogeosciences, Japan Agency for Marine-Earth Science and Technology, 2-15 Natsushima-cho, Yokosuka 237-0061, Japan

N. O. Ogawa
e-mail: nanaogawa@jamstec.go.jp

N. Ohkouchi
e-mail: nohkouchi@jamstec.go.jp

T. Kadono
School of Medicine, University of Occupational and Environmental Health, 1-1 Iseigaoka, Yahata, Kitakyusyu 807-8555, Japan
e-mail: kadono@med.uoeh-u.ac.jp

K. Kurosawa (✉)
421, 4th building, 2-17-1, Tsudanuma, Narashino, Chiba 275-0016, Japan
e-mail: kosuke.kurosawa@perc.it-chiba.ac.jp

Stribring and Miller 1986), photochemistry driven by ultraviolet (UV) light from the Sun (Zahnle 1986; Sekine et al. 2003), and meteoritic impacts (Fegley et al. 1986; Mukhin et al. 1989). Lightning and photochemistry form HCN constantly. However, after HCN is produced it is also destroyed continuously; efficient accumulation would not have occurred in the redox-neutral early Earth atmosphere. In contrast, meteoritic impacts would cause episodic production and concentration of cyanides. Furthermore, the continuous existence of life may have begun 3.8 Ga at about the time of the termination of the heavy bombardment period as mentioned above (e.g., Tera et al. 1974; Schidlowski 1988; Rosing 1999). Thus, meteoritic impacts might have played a key role in the origin of life.

Chyba and Sagan (1992) classified organic supply mechanisms by meteoritic impacts into three categories: (1) atmospheric heating due to fast-expanding vapor plumes, (2) post-impact recombination, and (3) delivery of intact extraterrestrial organic matter in impactors. The first category was proposed by Fegley et al. (1986), whose thermo chemical calculations clearly showed the importance of meteoritic impacts to the cyanide inventory on the early Earth. A reducing atmosphere (C/O molar ratio >1) is, however, required for efficient HCN production because the production efficiency of HCN in a redox-neutral atmosphere (C/O molar ratio <1) is rather low (Chameides and Walker 1981; Miller and Schlesinger 1983; Fegley et al. 1986). Although the exact chemical composition of the early planetary atmosphere is still a matter of controversy (e.g., Kasting 1990, 1993; Sagan and Chyba 1997; Hashimoto et al. 2007; Schaefer and Fegley 2010; Zahnle et al. 2011), recent theories for planetary formation suggest that a highly reducing atmosphere may not occur with the presence of a deep magma ocean (e.g., Hirschmann 2012), which likely form during the final stage of planetary accretion through giant impacts (e.g., Canup 2004). Subsequently, the early atmosphere will be oxidized due to the hydrodynamic escape of hydrogen driven by intense UV radiation from the young Sun (e.g., Kulikov et al. 2007). Furthermore, volcanic gases on the early Earth should have been redox-neutral (N_2–CO_2–H_2O) given the oxidation state of Hadean mantle at 4.35 Ga is similar to the present-day mantle (Trail et al. 2011). Thus, atmospheric heating due to meteoritic impacts was not likely to have been the dominant process in cyanide production on the early Earth. The second process was experimentally studied by Gerasimov et al. (1998) and Mukhin et al. (1989). These authors used laser pulse heating techniques to simulate the post-impact chemistry in vapor plumes. An unexpectedly large amount of oxidized gases, such as CO and CO_2, were detected along with a small amount of HCN using a gas chromatograph mass spectrometer (GCMS). Gerasimov et al. (1998) and Mukhin et al. (1989) concluded that oxygen released from thermally decomposed silicates efficiently oxidized carbon species to CO and CO_2. In this process, the amount of HCN produced is limited by the nitrogen content of the impactors. Nitrogen in chondritic material is highly depleted compared with microbial biomass (e.g., Wasson and Kallemeyn 1988; Chapin et al. 2008; Sugita and Schultz 2009). The final process was studied by hydrocode calculations (e.g., Pierazzo and Melosh 2000) and shock recovery experiments (Blank et al. 2001). Given that carbonaceous chondrites contain complex organic molecules (e.g., Hayatsu and Anders 1981; Cronin et al. 1988; Cooper et al. 2001; Pizzarello 2012), these materials may have delivered organic compounds to the early Earth if they survived the impact shocks. Hypervelocity oblique impact experiments (Schultz and Gault 1990) and the hydrocode calculations (Pierazzo and Melosh 2000) indicate that a large fraction of the impactor does not experience an extremely high shock pressure at low-angle oblique impacts. However, subsequent aerodynamic heating after oblique impacts must be considered to determine the fate of organic matter in meteorites. When hypervelocity oblique impacts occur, a large fraction of the impactor does not undergo vaporization but retains a downrange motion at velocities comparable to the initial impact velocity (Schultz and Gault 1990; Schultz and Sugita 1996), and this downrange-moving material suffers intense heating due to aerodynamic ablation (Sugita and Schultz 2003a). Hence, the vast majority

of the organic molecules in impacting carbonaceous chondrites are expected to have thermally decomposed, even if they survived the impact shock (Sugita and Schultz 2009), although a small but considerable fraction of organic matter at a small translational velocity to the ground may have been supplied to the surface of the early Earth (e.g., Blank et al. 2001).

In this study, we focus on the fate of the destroyed organic matter, which is most of the meteoritic organic molecules delivered to the Earth and planets with an atmosphere, due to aerodynamic heating after oblique impacts. Previous impact experiments showed that CN radicals were produced around fast moving, fine-grained projectile fragments from carbon in the impactor and nitrogen in the ambient gas (Sugita and Schultz 2009). This implies that impact-induced aerodynamic interactions are likely to produce a local and transient chemical environment that favors efficient cyanide production (Sugita and Schultz 2009). Hence, it is possible that destroyed organic matter from meteorites due to aerodynamic ablation is converted to cyanides via subsequent chemical reactions in the ablation vapor and its wake. However, the chemical composition and abundances of the final chemical products have not been well studied as the emission spectroscopy used in Sugita and Schultz (2009) is unable to quantify the chemical composition at a quenching temperature. The CN radicals may react with water vapor in an ambient atmosphere and generate HCN and nitrile compounds, but they may also be converted to CO and NO through oxidation by CO_2 in the ambient atmosphere. Thus, quantitative measurements of the conversion ratio from vaporized carbon to HCN in a redox-neutral atmosphere are necessary to assess the role of mid-size impacts to cyanide inventory. It should be noted that a large impactor (>10 km) does not interact with an ambient atmosphere efficiently because its size is larger than the scale height of the atmosphere (~8 km). As such, we studied relatively small-scale impact phenomena where the size of the impactor is 0.1–1 km.

In this study, to evaluate cyanide production processes in early Earth's atmospheres due to mid-size impactors (0.1–1 km in diameter), we have investigated impact-driven aerodynamic ablation by hypervelocity impacts and laser ablation. A series of laser ablation experiments were conducted to investigate the chemical compositions of the final products in the gas-and condensed-phase after laser ablation. The effects of oxidation by CO_2 on the amount of HCN in the final chemical products were investigated over a wide range of CO_2 mixing ratios. Also, we conducted hypervelocity oblique impact experiments to confirm that laser ablation can simulate CN production processes due to aerodynamic ablation after oblique impacts based on diatomic molecular emission.

First, we describe the impact and laser experiments in detail (Section 2) and the results are presented (Section 3). Then, in Sections 4.1 and 4.2, we show that laser ablation of a graphite target in a N_2-rich gas can simulate impact-induced aerodynamic ablation. The advantage of impact-induced aerodynamic ablation on the HCN production compared with the other impact-driven processes is discussed in Section 4.3. Based on the experimental results, the implications of our results for the cyanide inventory on the early Earth (the column density of HCN on the surface of the early Earth after a mid-size oblique impact) are discussed in Sections 4.4 and 4.5. Finally, the conclusions are presented in Section 5.

Impact and Laser Experiments

We conducted two types of experiments; hypervelocity impacts and laser ablation. In the two-stage gas-gun experiments, chemical analyses of the final chemical products are difficult to make due to chemical contamination from the acceleration gas and gun debris. Although Kurosawa et al. (2012) developed an experimental procedure to measure inorganic

gas-phase products after an impact in an open system using a two-stage light gas gun, analysis of minor organic compounds of ppm level is still technically challenging because they used a plastic diaphragm to minimize the intrusion of the acceleration gas into an experimental chamber. Thus, a Nd: YAG laser was used to investigate the fate of impact-generated CN radicals in this study. High-temperature CN radicals can be produced by laser irradiation of a graphite target in a N_2-rich gas via fluid instability near the boundary between the carbon vapor plume and the ambient gas (e.g., Vivien et al. 1998; Sharma and Thareja 2005; Kurosawa et al. 2009). Given that the laser pulse penetrates through a glass view port, experiments can be conducted in a closed vacuum chamber. The final chemical products can then be measured to high accuracy with little risk of chemical contamination (e.g., Mukhin et al. 1989; McKay and Borucki 1997; Gerasimov et al. 1998; Ohno et al. 2004; Ishibashi et al. 2006, 2013). The differences between the thermodynamic state of impact-and laser-generated CN radicals, however, has not been well studied. Chemical reactions are strongly dependent on the thermodynamic path and, as such, differences should be examined by conducting impact experiments prior to applying the results of laser experiments to real impact phenomena. Given this, the fate of hot CN radicals was investigated in detail using laser ablation.

Hypervelocity Oblique Impact Experiments

The two-stage light gas gun with 7 mm bore diameter (Physics Applications Inc.) in the Space Plasma Laboratory in Institute of Space and Astronautical Science (ISAS) of the Japan Aerospace and Exploration Agency (JAXA) was used for hypervelocity oblique impact experiments. We carried out high-resolution spectroscopic observations to determine both the vibrational structure and translational–rotational temperature of impact-generated CN radicals.

Experimental Setup

Our experimental system consists of four components; a two-stage light gas gun, a vacuum chamber, a gas cylinder of N_2, and a high-speed optical spectrometer using a intensified charge-coupled device (ICCD) camera (Acton, SpectraPro 2750 and Roper Scientific, PI-MAX). Figure 1a is a schematic diagram of the experimental system. The focal length of the spectrometer is 750 mm. We used two gratings with different groove densities. Wavelength resolutions and coverage are about 0.6 nm and 0.03 nm (full width at half maximum; FWHM) and 200 nm and 10 nm for the gratings with groove densities of 150 and 2,400 grooves/mm, respectively. Calibration experiments for both wavelength and irradiance were carried out with a mercury lamp (Electro-Technic Inc., MODEL SP 200) and a NIST-traceable tungsten halogen quartz lamp (ORIEL corporation, Model 63355), respectively. A photomultiplier tube was used to detect muzzle flash and to provide a trigger for the measurement system.

Experimental Conditions

Polycarbonate sphere (7 mm in diameter) and copper block (50 mm×100 mm×20 mm) were used as the projectile and target, respectively. Nitrogen was used as the ambient gas in the chamber. The total pressure in the chamber was fixed at 30 mbar. The impact angle was fixed at 30° from the horizontal and the impact velocity was ~7 km/s. The diameter of the field of view (FOV) of spectroscopic observations was fixed at ~3 cm, and the exposure time of ICCD camera was fixed at 30 μs after impact.

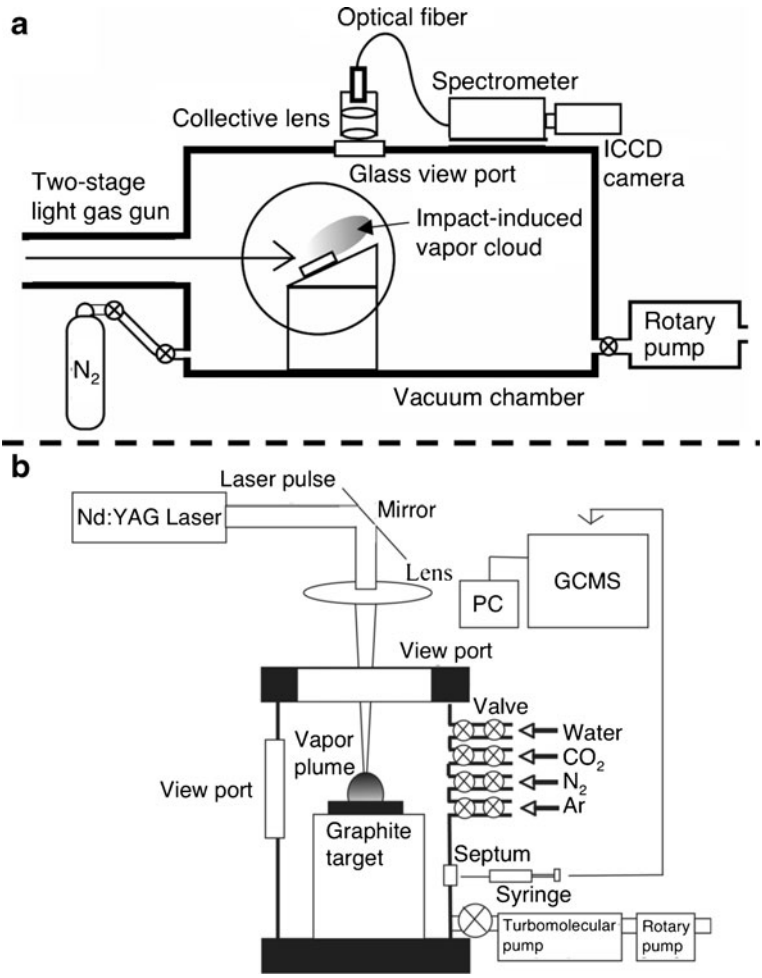

Fig. 1 A schematic diagram of the experimental system for impact (**a**) and laser experiments (**b**). Note that the glass view port at the side of the chamber for the laser experiments was used for spectroscopic observations in the study by Kurosawa et al. (2009)

Experimental Procedures

After a copper target was placed on the stage, the vacuum chamber was evacuated to a residual pressure of 8×10^{-2} mbar before each shot. N_2 gas was then introduced into the chamber before shooting a projectile into the target. An emission spectrum of self-luminous impact-induced vapor was recorded by the ICCD camera.

Laser Experiments

A Nd: YAG laser at the University of Tokyo was used to investigate the final chemical products. Two types of chemical analyses were conducted; mass spectrometry of the gas-phase products, and elemental analysis and infrared (IR) spectroscopy of the condensed-phase products deposited on a substrate. For the gas-phase products, we quantitatively

measured the amount of HCN per laser shot as a function of the partial pressure of CO_2 (hereafter referred to as P_{CO2}). The relative amounts of the other gas-phase products were measured based on the integrated peak area of the monitored ion current. For condensed-phase products, the mass contents of total nitrogen and carbon (hereafter referred to as *TN* and *TC*, respectively) were measured with an elemental analyzer. In addition, the effects of the partial pressure of N_2 (hereafter referred to as P_{N2}) on the chemical structure of the condensed products, such as the absorption depth of the C=N and C≡N bonds, were also investigated using a Fourier transform infrared spectrometer (FT-IR).

Experimental Setup

The system for laser experiments consists of a Nd: YAG laser, a vacuum chamber, gas cylinders, and a GCMS (Shimadzu Corporation, QP2010). A small tank filled with pure water was connected to the chamber to introduce water vapor up to a saturated vapor pressure of ~30 mbar. A gas chromatograph column suitable for inorganic and light organic gas analysis (Agilent Technologies, GS-Q) was used. The laser experimental system is shown schematically in Fig. 1b.

In order to collect the condensed products from the laser-generated ablation vapor, we placed a CaF_2 disk (2 mm thick, 25 mm diameter; IR Systems) at ~6 cm beside the laser spot on the target. To examine the effect of distance between the laser spot and the condensation disk, we conducted the same experiment with a disk placed at a different distance ~11 cm from the laser spot. Elemental analysis was performed with an online system comprising a Finnigan Delta Plus XP isotope ratio mass spectrometer coupled to a Flash EA1112 elemental analyzer (EA/IRMS system) at the Japan Agency for Marine-Earth Science and Technology (Ohkouchi et al. 2005). Infrared absorption spectroscopy was carried out with a FT-IR (Perkin Elmer, Spectrum 2000) at the University of Tokyo.

Experimental Conditions

A sintered graphite pellet (C=99.999 wt%; Kojundo Kagaku) was used as the target. The laser wavelength was 1,064 nm and the laser pulse width was ~13 ns. The energy of the laser pulse was fixed at ~380 mJ/pulse. The diameter of the laser beam on the target surface was ~2 mm, resulting in a laser intensity of 0.9 GW/cm^2, which was sufficient to evaporate graphite. The irradiation frequency of the laser pulse was fixed at 2 Hz. All laser experiments were conducted in a vacuum chamber with a volume of 890 mL. The vacuum chamber had four gas inlets in order to introduce a variety of gases individually. A manometer was used to adjust the partial pressure of each gas.

The experimental conditions for gas-phase chemical analysis are as follows. The total pressure in the chamber was fixed at 1,060 mbar. Two series of experiments were conducted. Firstly, four gas mixtures (Ar [N- and H-free], H_2O–Ar [N-free], N_2–Ar [H-free], N_2–H_2O–Ar) were used to examine the effects of the presence of H_2O and N_2 on HCN production. The partial pressures of N_2 and H_2O were fixed at 930 mbar and 30 mbar, respectively. Secondly, the effects of oxidation by CO_2 on the amount of HCN and the other products were investigated using N_2–CO_2–H_2O–Ar gas mixtures with different CO_2 mixing ratios. In order to examine the effects of P_{N2} on HCN yield, we used two values of P_{N2} (920 mbar and 500 mbar). P_{CO2} was varied from 0 mbar to 110 mbar and 0 mbar to 530 mbar, respectively. Argon gas was used to adjust the total pressure in the chamber to a constant value of 1,060 mbar. During the experiments, the temperature of the wall of the vacuum chamber was kept at 350 K to prevent water condensation.

The experimental conditions for condensate analysis are as follows. Water vapor was not used in condensate analysis to enhance the condensation of chemical products. The objective of the condensed-phase analysis was to examine whether fixation of CN bonds into the condensate occurred. Mass flow controllers and a vacuum pump were used to minimize changes in the chemical composition of the ambient gases. Flow-system experiments were necessary for the condensed-phase analyses because a large number of laser shots were necessary to collect a sufficient amount of condensed products for solid-phase chemical analyses. Necessary laser shots for condensed phase analyses is more than five times those for gas-phase analysis. We used N_2–CO_2–Ar gas mixtures with a variety of P_{CO2} and P_{N2} values. The equilibrium total pressure in the chamber was fixed at 13 mbar using Ar gas to adjust the total pressure in the chamber in the same way as the gas-phase analysis.

Experimental Procedures

A graphite target was placed on the stage in the chamber, and the position and the diameter of the laser beam on the target were adjusted. The vacuum chamber was then evacuated to ~10^{-6} mbar and the chamber wall heated to 350 K. The gas mixtures were then introduced into the vacuum chamber and laser irradiation started. As no clear signal could be detected after a single laser shot during chemical analyses, 300 and 1900 laser shots were accumulated for gas-and condensed-phase analysis, respectively. If the same point on the target was irradiated with the laser beam repeatedly for a long time, it gradually forms a pit, which would affect the condition of the carbon vapor and CN radicals. Thus, the position of the laser focus point on the target was changed continuously. After laser irradiation, 1 mL of the final gas-phase products was sampled using a syringe and analyzed with the GCMS. For condensed-phase analysis, the CaF_2 substrate was removed from the chamber and analyzed by FT-IR in order to measure the absorption depth due to nitrogen-bearing chemical bonds, such as C=N and C≡N, in the products. Following this, 1–10 mg of the condensed products were transferred into pre-cleaned capsules and introduced into the EA/IRMS system. The amounts of N_2 and CO_2 produced in the EA/IRMS system yielded the *TN* and *TC* in the condensed products, respectively.

Experimental Results

The main result of our study is the quantification of the conversion ratio from vaporized carbon to gaseous HCN as a function of P_{CO2}. Our spectroscopic results support the applicability of the conversion ratio obtained by laser ablation to real impact phenomena.

Spectroscopic Comparison Between Impact-and Laser-Induced Vapor Clouds

We obtained emission spectra from impact-generated ablation vapors produced at ~7 km/s under 30 mbar of N_2. Figure 2 shows high-speed photographs during impacts. A fast downrange-moving, self-luminous component was observed. Figure 3 is a comparison of the spectral outlines between impact-and laser-generated ablation vapors. The main emission source in both experiments is molecular emission from CN and C_2. The observed spectrum produced by impacts results in a strong continuum emission. The radiation source of the continuum emission is expected to be impact-generated fine-grained fragments, including melt droplets (Sugita and Schultz 2003b). Although strong continuum emission was not observed in laser experiments, the observed spectrum produced by impacts is similar to that

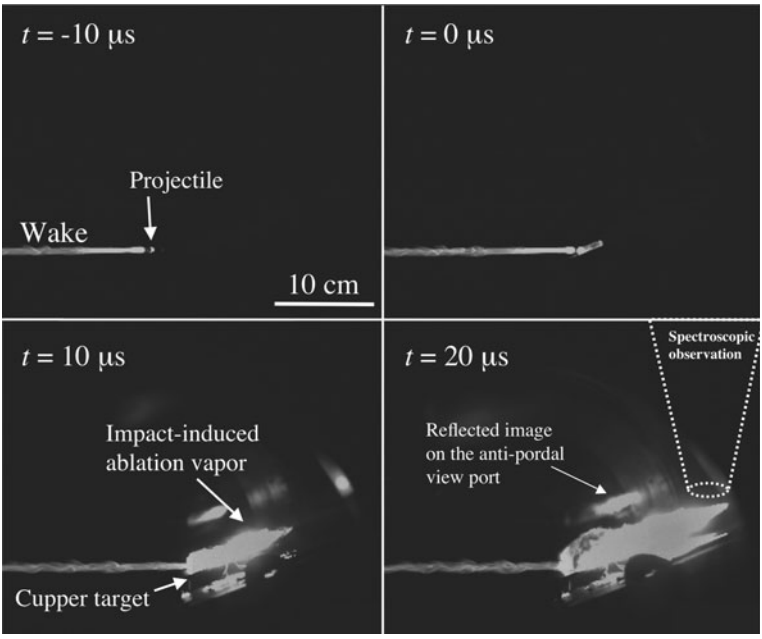

Fig. 2 High-speed photographs of a polycarbonate impact into a Cu target within 30 mbar of N_2 gas. The distance between the impact point and the field of view of the spectroscopic observation is 12 cm (the projectile is 0.7 cm in diameter)

produced by laser ablation. The blackbody temperature was estimated by Planck function fitting to the continuum spectra.

We then compared the vibrational state of CN in both types of vapor clouds. Figure 4 shows high-resolution spectra from impact (Fig. 4a) and laser ablation (Fig. 4b) experiments. For comparison, a theoretical synthetic spectrum in thermal equilibrium (7,000 K) is also shown in Fig. 4c. The computer software package SPRADIAN (structured package for radiation analysis) (Fujita and Abe 1997) was used to calculate the theoretical synthetic spectrum. This comparison clearly shows that the impact-generated CN radicals were not in vibrational equilibrium in the same way as the laser-generated one reported by the previous study (Kurosawa et al. 2009), because the ratio of intensities of different band heads deviates strongly from a Boltzmann distribution. The characteristic time scale of CN band emission due to transition from the upper quantum state to the lower one is ~60 ns (Hertzberg 1950), which is much shorter than the relaxation time scale for the vibrational state of ~1 μs (Slack 1976). Thus, the observed non-equilibrium CN is evidence for fast CN production via vaporized carbon and nitrogen from the ambient atmosphere in both the impact-and laser-generated ablation vapors.

Finally, we quantitatively compared the translational–rotational temperature of CN and C_2 in both vapors. The band-tail fitting method (Kurosawa et al. 2009) was used to measure the translational–rotational temperature for CN and C_2 as this method can be applied to molecular spectra from matter in vibrational non-equilibrium. The results of band-tail fitting for CN and C_2 in the impact vapor are shown in Fig. 5. The band-tails of the observed spectra and best-fit synthetics are in good agreement. Table 1 shows the summary of the obtained translational–rotational temperatures for CN and C_2 and blackbody temperatures. The translational–rotational temperatures of C_2 are nearly equal to the blackbody temperatures. This coincidence between C_2 translational-rotational and blackbody temperatures is consistent with the previous impact

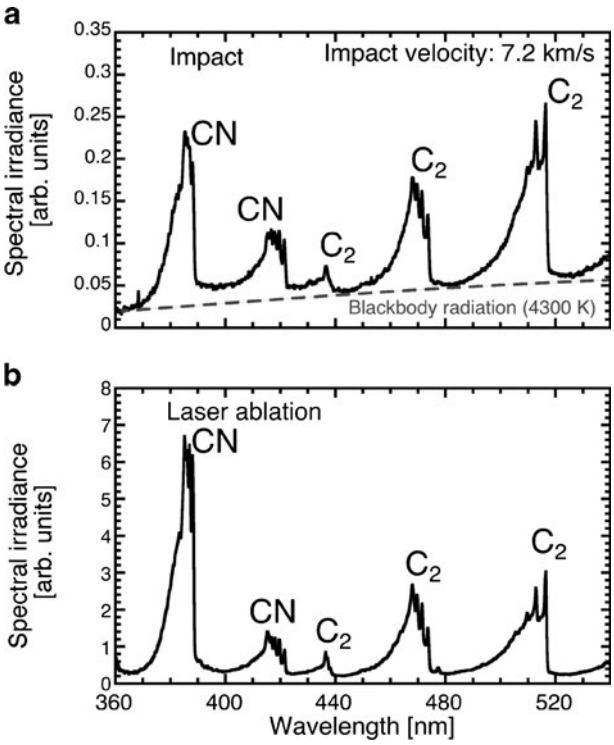

Fig. 3 A spectral comparison between impact-(**a**) and laser-induced (**b**) ablation vapors. The identified molecular emissions are shown on the figure. The emission spectrum from the laser-generated ablation vapor is taken from Kurosawa et al. (2009). The best-fit Planck function is also shown in (**a**)

experiments by Sugita and Schultz (2003a). The initial translational–rotational temperatures (2–4 μs) of CN and C_2 produced by laser ablation at 0.9 GW/cm^2 are also shown in Table 1. The translational–rotational temperatures of both CN and C_2 produced by impacts at ~7 km/s are similar to those produced by laser ablation. In both experiments, the translational–rotational temperature of CN is ~2,000 K higher than that of C_2. This difference is caused by the conversion of kinetic energy from the ablation vapor into the internal energy of CN due to aerodynamic deceleration. This phenomena is widely known as "collisional heating" in laser ablation studies (e.g., Wee and Park 1999).

The above spectroscopic results that both non-equilibrium CN and coincidence between translational-rotational temperature of impact-and laser-generated ablation vapor strongly suggest that very similar physical and chemical conditions occur in the two different types of experiments. This will allow us to use laser experiments to examine the chemical consequences of impact-generated high-temperature CN radicals observed by Sugita and Schultz (2009). The validity of using a simulation of aerodynamic interaction after oblique impacts by laser ablation is also discussed in Sections 4.1 and 4.2.

Cyanide Production due to Laser Ablation in a Redox-Neutral Gas Mixture

The Effects of the Composition of the Ambient Gas Mixture on HCN Production

Four gas mixtures were used to investigate the effects of the composition of the gas mixture on HCN production. We found that HCN formation by chemical reactions between laser-induced hot CN radicals and N_2 and H_2O in an ambient atmosphere occurs as follows. Figure 6 shows chromatograms, which are the total ion currents as a function of retention time, obtained with

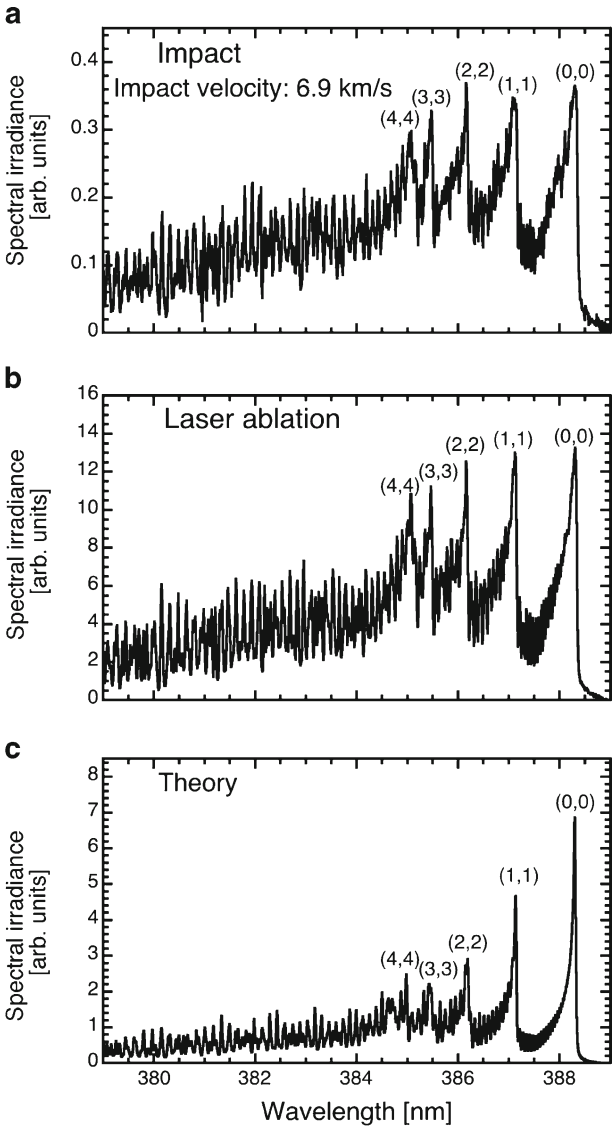

Fig. 4 High-resolution emission spectra of the CN Violet band system. The emission spectrum from the laser-induced ablation vapor is taken from Kurosawa et al. (2009). The vibrational quantum numbers for each band head are shown in the figure

four gas mixtures after 300 laser shots. The experimental results are also given in Table 2. These results clearly indicate that the chemical composition of the gas-phase products strongly depends on the composition of the ambient gas mixture. If a gas mixture included H_2O, hydrocarbons were formed. If a gas mixture included N_2, cyanide compounds were formed. In an Ar gas, HCN was not formed, and only a small peak of C_2H_2 was detected. C_2H_2 is likely to have formed by chemical reactions between the laser-induced carbon vapor and a contaminant gas (e.g., water vapor and/or hydrocarbons) in the chamber. In a H_2O–Ar gas mixture, some hydrocarbons were detected, such as C_2H_4, C_2H_2, and C_4H_2, but HCN was not detected. In a N_2–Ar gas mixture, a large peak of C_2N_2 and a small peak of HCN was detected. The detected HCN was possibly formed by chemical reactions between hot CN and contaminant gases in the chamber. In a N_2–H_2O–Ar gas mixture, a large peak of HCN, C_2H_2, and C_2N_2, and

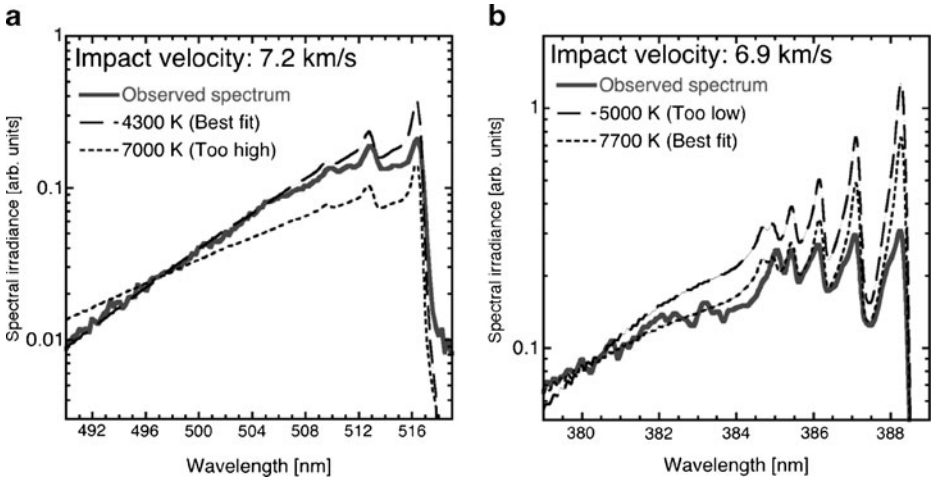

Fig. 5 The results of band-tail fitting for impact-induced C_2 (b) and CN (b). Note that the observed spectrum in (b) is smoothed by Gaussian convolution to reduce the effective spectral resolution. The smoothing is necessary because it is difficult to reproduce the fine structure of the band system, such as the exact wavelength of each rotational line in synthetic calculations

a small peak of nitrile compounds, such as C_2H_3N, C_3H_3N, and C_3H_5N, along with some hydrocarbons, such as C_2H_4, C_2H_6, and C_4H_2 were detected. It was possible to monitor the ion current for selected mass numbers (M/Z) using the GCMS and calculate the integrated peak area for HCN (M/Z=27). Hereafter, the ion current for a specific mass number is referred to as the monitored ion current (MIC). The integrated peak area of HCN in the N_2–H_2O–Ar gas mixture is about 7 times greater than in the N_2–Ar gas mixture. These results clearly indicate that whether or not the ambient atmosphere contains N_2 and H_2O controls the HCN yield, strongly suggesting that HCN is produced via chemical reactions between laser-generated carbon vapor and the ambient gas mixture, not contaminant gases in the chamber.

The Effects of Oxidation by CO_2 on HCN Yield

The results of gas-phase chemical analysis in N_2–H_2O–CO_2–Ar gas mixtures over a range of CO_2 mixing ratios were described in this section. We present the empirical conversion ratio

Table 1 Summary of the impact experiment results

Shot number	Grating [grooves/mm]	Impact velocity [km/s]	Temperature [K]		
			CN	C_2	Blackbody
205	150	7.17	–	4,800±250	4,300
207	2,400	6.9	7,700±190	–	–
		Laser intensity [GW/cm^2]			
Laser	150	0.9	–	4,600±300[a]	–
Laser	2,400	0.9	7,500±300[a]	–	–

[a] Data taken from Kurosawa et al. (2009). The time window for spectroscopic observations was 2–4 μs after laser irradiation

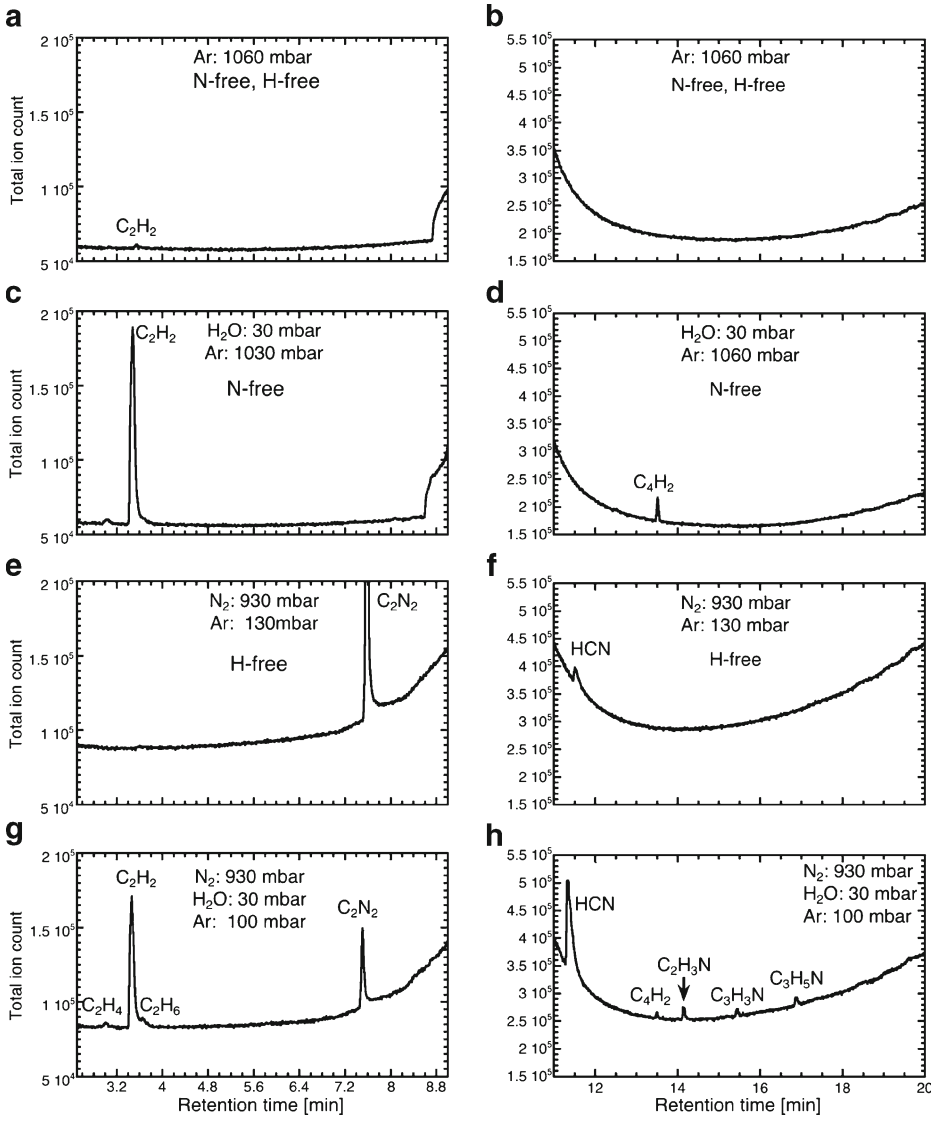

Fig. 6 Chromatograms with four types of gas mixtures. The compositions of the ambient gas mixtures are shown on the figure. The retention time for HCN is 11–12 min under these conditions. The chromatogram between 9 and 11 min is not shown because of a large peak of H_2O that appears at this time

from C to HCN as a function of P_{CO2}. Figure 7a shows the MIC for HCN with a range of P_{CO2} from 0 mbar to 530 mbar. The integrated peak area for HCN strongly depends on P_{CO2}. To convert from the integrated peak area to the molar mixing ratio of HCN in the produced gases, a sensitivity calibration for the GCMS was conducted with standard gases with a variety of HCN mixing ratios (Fig. 7b). Note that the calibration curve is non-linear under our experimental condition because HCN has a strong polarity. The accuracy of the calibration is about 6 % from 15 ppm to 87 ppm HCN. The detection limit of HCN is approximately 4 ppm under the experimental conditions used in our study. The HCN

Table 2 The results of GCMS measurements with four different gas mixtures

Gas mixture	Ethylene C_2H_4	Acetylene C_2H_2	Ethane C_2H_6	Butadiyne C_4H_2	Acetonitrile C_2H_3N	Propenitrile C_3H_3N	Propanenitrile C_3H_5N	Cyanogen C_2N_2	Hydrogen cyanide HCN	N_{HCN} [nmol/pulse]	ϕ mol%
Ar	N. D.	9.6E+03	N. D.	N. D.	N. D.	N. D.	N. D.	N. D.	N. D.	<0.4	<0.08
H_2O-Ar	N. D.	5.5E+05	8.0E+03	7.5E+04	N. D.	N. D.	N. D.	N. D.	N. D.	<0.4	<0.08
N_2-Ar	N. D.	N. D.	2.2E+03	N. D.	2.7E+03	N. D.	N. D.	8.0E+05	1.8E+05	5.3	1.1
N_2-H_2O-Ar	8.1E+03	3.5E+05	1.0E+04	1.7E+04	4.4E+04	1.2E+04	3.0E+04	1.6E+05	1.3E+06	14	2.8

The integrated peak area of the monitored ion current for each species, HCN production per laser pulse, and the conversion ratio ϕ from C to HCN are shown. "N. D." denotes not detected

production per laser pulse (N_{HCN}) can be calculated based on the molar mixing ratio, chamber volume, number of laser shots, and the ideal gas equation of state. We assumed that the temperature of the produced gases is equal to the temperature of the chamber wall (350 K) in this calculation. Figure 7a shows N_{HCN} as a function of P_{CO2} and P_{N2}. N_{HCN} decreases systematically as P_{CO2} increases, and a higher P_{N2} leads to larger N_{HCN}. HCN production could not be detected under P_{CO2} values of 530 mbar (i.e., N_2/CO_2 molar ratio <1). In order to apply the experimental results to real impact phenomena, the conversion ratio (ϕ) of vaporized carbon to gaseous HCN is determined as follows. To estimate the total amount of vaporized carbon N_c, we assumed that the shape of the vaporized region produced by laser ablation is cylindrical and the depth is equal to the wavelength of the laser pulse (~1 μm), which is a characteristic scale of energy deposition of laser irradiation. As a result, the amount of vaporized carbon (N_C) is estimated to be ~500 nmol/pulse. The conversion ratio is given by $\phi = N_{HCN}/N_C$. Figure 8b shows ϕ as a function of P_{CO2}. The conversion ratio varies from 0.1 mol% to 2 mol% over P_{CO2}=0–390 mbar. Although ϕ systematically decreases as P_{CO2} increases, a significant fraction (0.1–1 mol%) of vaporized carbon is converted to HCN in redox-neutral gas mixtures containing as much as a few hundred mbar of CO_2. It is noted that the HCN energy yield obtained in our experiments is 10^{15}–10^{16} molecules/J, which is ~4 orders of magnitude greater than that in simple gas-phase calculations due to Chameides and Walker (1981) for a redox-neutral atmosphere (i.e., C/O molar ratio <1). This suggests that the composition of vapor plumes generated by ablation stay reduced throughout their evolution despite their mixing with ambient atmospheric gas. The integrated peak area for each identified species, HCN production, and ϕ are given in Table 3. Hydrocarbons, cyanogen, and nitrile compounds were also produced within the redox-neutral gas mixtures, although the integrated peak area for these species decreases as P_{CO2} increases. Quantification of the amount of these species is a potential avenue for future research.

Chemical Analyses of the Condensates

The conversion ratio from vaporized carbon to gaseous HCN is only 0.1–2 mol% as shown in the previous section. The fate of other carbon, including spectroscopically detected CN radicals,

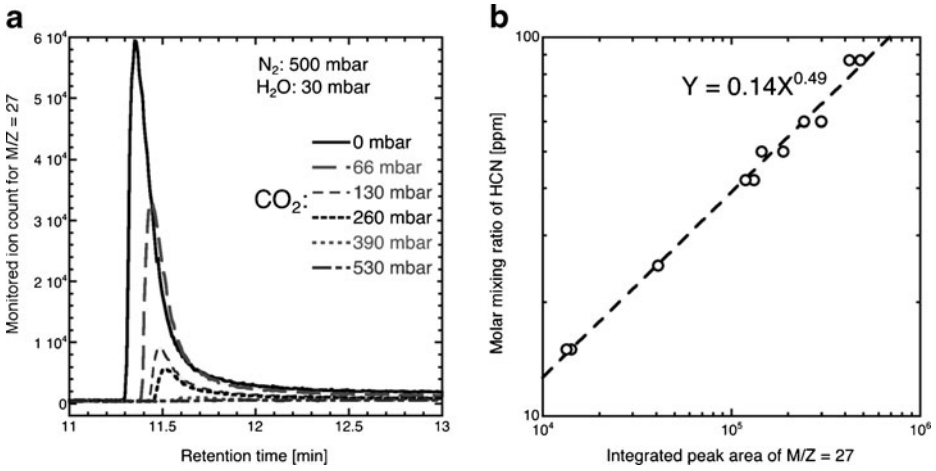

Fig. 7 **a** Monitored ion current for HCN (M/Z=27) as a function of the partial pressure of CO_2. **b** The results of the sensitivity calibration for the GCMS

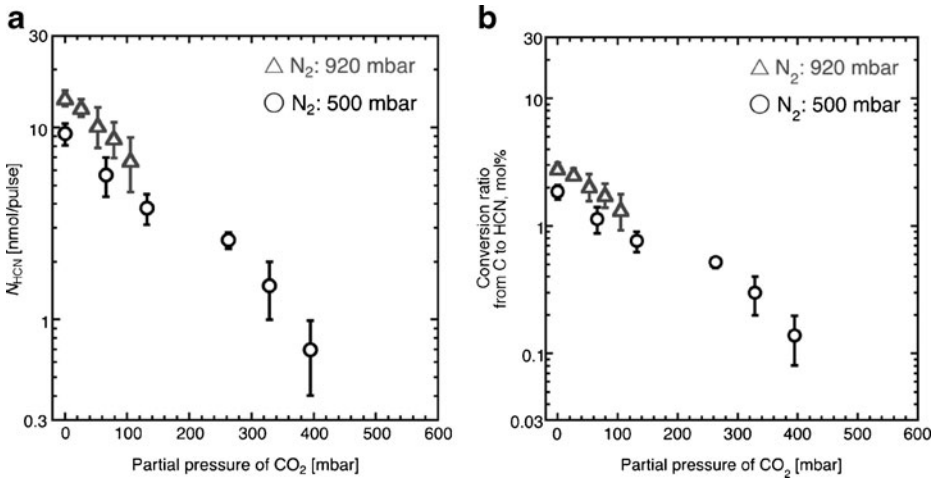

Fig. 8 The amount of HCN produced per laser shot as a function of the partial pressure of CO_2 (**a**) and the conversion ratio ϕ of vaporized carbon to gaseous HCN (**b**). Squares and circles indicate the data obtained under P_{N2}=920 mbar and 500 mbar, respectively. The arrows indicate the detection limit under the experimental conditions

in the ablation vapor is still uncertain. In this section, we examine whether the vaporized carbon is fixed into a condensed phase by forming CN bond or not. The main result of the chemical analyses of the condensed phase is identification of the dependence of both *TN* and the absorption depth of the CN bond of the condensed products on P_{N2}. We found that nitrogen in the gas phase was efficiently fixed into the solid products condensed from the laser-induced ablation vapor. The absorption depth of the CN bond also increases as P_{N2} increases.

The elemental analysis results of the condensed products are shown in Fig. 9. These results show that the chemical composition strongly depends on that of the ambient gas. The condensed products were not observed in the laser irradiation experiments onto a graphite target in CO_2 gas, suggesting that most of the carbon in the laser-generated ablation vapor is oxidized to CO gas by reactions with ambient CO_2 gas. When N_2 was used as the ambient gas, *TN* reaches up to ~10 wt% in the condensed products. This suggests that nitrogen in the gas phase is incorporated into the condensed phase (*TN* ~10 wt%) via chemical reactions with the laser-induced ablation vapor.

Infrared spectroscopy measurements of the condensed products also support the hypothesis that N_2 in the gas phase is incorporated into the condensed products by reacting with C in the laser-generated ablation vapor. Figure 10a shows IR absorption spectra of the condensed products formed by laser irradiation of graphite under various gas mixtures. This figure shows that the depth of the absorption bands around 2,200 cm^{-1} increase with the P_{N2}. This band corresponds to C≡N and −N=C=N bonds (e.g., Rao 1963), and also often seen in Titan tholin simulants synthesized in laboratory experiments under N_2-rich atmospheric conditions (e.g., Imanaka et al. 2004). The depth of the absorption bands around 1,600 cm^{-1} in the IR absorption spectra, which correspond to C=N bonds, also increase with P_{N2}. Figure 10b shows that the effects of the distance between the laser spot and the CaF_2 disk on IR spectra. This result clearly shows the distance does not affect the spectral shape qualitatively. Both absorption bands around 2,200 and 1,600 cm^{-1} contain contributions from the presence of C≡C and C=C bonds, respectively, in the condensed products. Therefore, the increase in the absorption depths may not only be due to the formation of C≡N and C=N bonds. Nevertheless, the observed systematic

Table 3 Results of GCMS measurements with N_2–H_2O–CO_2–Ar gas mixtures over a range of CO_2 mixing ratios

P_{CO2} [mbar]	P_{N2} [mbar]	Ethylene C_2H_4	Acetylene C_2H_2	Ethane C_2H_6	Butadiyne C_4H_2	Acetonitrile C_2H_3N	Propenitrile C_3H_5N	Cyanogen	C_2N_2	Hydrogen cyanide HCN	N_{HCN} [nmol/pulse]	ϕ mol%
0	920	8.1E+03	3.5E+05	1.3E+04	1.7E+04	4.4E+04	1.2E+04	3.0E+04	1.6E+05	1.3E+06	14	2.8
0	920	4.9E+03	2.4E+05	9.2E+03	7.8E+03	4.6E+04	1.2E+04	3.6+04	2.1E+05	1.1E+06	13	2.6
26	920	6.1E+03	3.1E+05	1.2E+04	1.1E+04	2.4E+04	7.5E+03	1.8E+04	6.2E+04	9.1E+05	12	2.4
26	920	7.3E+03	3.5E+05	1.1E+04	1.0E+04	2.7E+04	7.5E+03	2.1E+04	4.5E+04	1.0E+06	12	2.4
53	920	6.1E+02	2.3E+05	9.7E+03	1.1E+04	1.5E+04	4.2E+03	1.2E+04	1.3E+04	4.3E+05	8.2	1.64
53	920	7.0E+03	3.0E+05	9.0E+03	1.1E+04	2.0E+04	6.0E+03	2.0E+04	2.4E+04	7.9E+05	11	2.2
79	920	6.5E+03	3.0E+05	8.4E+03	1.3E+04	1.7E+04	4.8E+03	1.0E+04	7.2E+03	5.3E+05	9.1	1.82
79	920	3.1E+03	2.1E+05	2.2E+03	7.8E+03	1.3E+04	4.0E+03	5.0E+03	1.2E+04	3.5E+05	9.1	1.82
110	920	5.8E+03	1.7E+05	2.3E+03	1.1E+04	1.4E+04	4.3E+03	7.7E+03	8.5E+03	3.0E+05	6.8	1.36
110	920	4.9E+03	1.8E+05	3.7E+03	1.0E+04	1.6E+04	4.0E+03	1.0E+04	8.9E+03	3.4E+05	7.3	1.46
0	500	N. D.	1.9E+05	7.4E+03	1.4E+03	3.4E+04	5.7E+03	3.4E+04	1.1E+05	7.3E+05	11	2.2
0	500	N. D.	1.3E+05	N. D.	N. D.	2.8E+04	2.2E+03	2.6E+04	9.6E+04	5.8E+05	9.5	1.9
66	500	7.3E+03	1.3E+05	9.4E+03	4.9E+03	1.4E+04	2.3E+03	3.4E+04	1.1E+05	7.3E+05	11	2.2
66	500	N. D.	1.3E+05	5.9E+03	5.3E+03	7.5E+03	1.5E+03	6.1E+03	6.2E+03	1.9E+05	5.4	1.08
130	500	N. D.	6.9E+04	N. D.	4.0E+03	8.4E+03	1.5E+03	N. D.	5.7E+03	7.7E+04	3.5	0.7
130	500	N. D.	7.6E+04	N. D.	4.3E+03	9.1E+03	2.3E+03	N. D.	8.7E+03	1.3E+05	4.6	0.92
260	500	N. D.	7.6E+04	N. D.	4.3E+03	9.1E+03	2.3E+03	N. D.	2.4E+03	5.7E+04	3	0.6
260	500	N. D.	6.4E+04	N. D.	6.8E+03	8.3E+03	1.3E+03	N. D.	2.4E+03	4.4E+04	2.7	0.54
330	500	N. D.	4.4E+04	N. D.	5.2E+03	4.9E+03	1.2E+03	N. D.	1.6E+03	1.3E+04	1.5	0.3
330	500	N. D.	6.2E+04	N. D.	8.5E+03	6.8E+03	2.0E+03	N. D.	N. D.	4.2E+04	2.6	0.52
400	500	N. D.	4.6E+04	N. D.	7.8E+03	4.9E+03	N. D.	N. D.	N. D.	1.2E+04	1.4	0.28
400	500	N. D.	4.6E+04	N. D.	8.1E+03	4.6E+03	N. D.	N. D.	N. D.	3.5E+03	0.78	0.156
530	500	3.1E+03	3.6E+04	N. D.	8.9E+03	3.3E+03	N. D.	N. D.	N. D.	N. D.	<0.4	<0.08

The partial pressure of H_2O was fixed at 30 mbar in this series of experiments. In the same way as Table 2, the integrated peak area of the monitored ion current for each species, HCN production per laser pulse, and the conversion ratio ϕ from C to HCN are shown. "N. D." denotes not detected

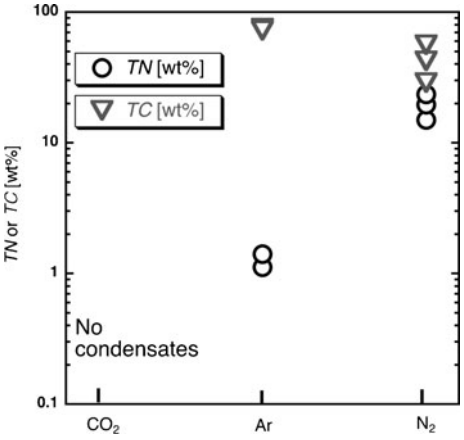

Fig. 9 The results of elemental analysis for condensed phase products. The mass contents of total nitrogen and carbon are abbreviated as *TN* and *TC*

changes in the depth of these absorption bands with P_{N2} strongly support the presence of C≡N, C=N, and −N=C=N bonds in the condensed products formed by laser irradiation under N_2-containing gas mixtures.

Discussion

In this section, we discuss whether laser ablation can simulate aerodynamic ablation processes due to mid-size impacts, based on the results of impact experiments in Section 4.1, the effect of the scale difference outlined in Section 4.2, the comparison with other impact-driven processes

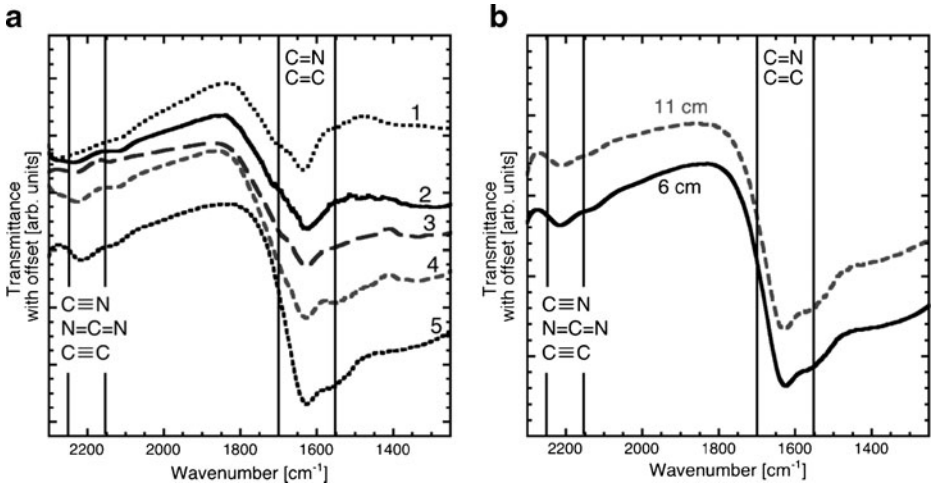

Fig. 10 The results of infrared spectroscopy for condensates: The effects of the composition of ambient gases (a) and the distance between the laser spot and the CaF_2 substrate. The positions of the absorption bands of C≡N, −N=C=N, and C=N are shown. In (**a**), the numbers indicate the difference in the composition of the ambient gas flow: (1) Ar=13 mbar, (2) N_2=3 mbar, CO_2=3 mbar, and Ar=7 mbar, (3) N_2=6 mbar, CO_2=3 mbar, and Ar=5 mbar, (4) N_2=10 mbar and CO_2=3 mbar, (5) N_2=13 mbar. In experiments (**b**), we chose 13 mbar of N2 as the ambient gas flow. The distances between the laser spots and the substrate of each experiments are shown in the figure

in Section 4.3, and the dominant impactor type during the heavy bombardment period in Section 4.4. Finally, we consider the implications of our study for the early Earth in Section 4.5.

The Thermodynamic State of the Impact-and Laser-Generated Ablation Vapor

The impact experiment results show that laser-and impact-generated ablation vapors qualitatively exhibit two similarities in terms of spectral shapes and the nature of vibrational non-equilibrium, and quantitatively are in accordance with translational–rotational temperatures.

Here, we discuss the location of CN formation and the pressure of impact-and laser-generated ablation vapors. The equilibration time scale of the translational temperature is very short (~20 ns for N_2 at 10^5 Pa) (Fujita 2007). Thus, the observed CN and C_2 in impact experiments are likely to be spatially separated as the translational temperature of CN is much higher (~2,000 K) than that of C_2. This situation is similar to laser-generated CN and C_2 (e.g., Thareja et al. 2002). We then consider the pressures of both vapors. Although we did not measure the pressure of the impact-generated ablation vapors, it should be controlled by aerodynamic ram pressure ($\sim\rho_a v^2$, where ρ_a and v are the atmospheric density and translational velocity of the vapor, respectively) from the colliding atmospheres. The translational velocities of both vapors are ~10 km/s (e.g., Schultz and Gault 1990; Kadono et al. 2002) and so the pressures of both vapors are expected to be similar. It is noteworthy that the typical peak shock pressure at impacts >100 GPa is much higher than the aerodynamic ram pressure (~0.1 GPa) at a translational velocity of 10 km/s and an atmospheric density of 1 kg/m^3. The possible production and subsequent chemical reaction processes of hot CN radicals due to both impacts and laser ablation are as follows. Gaseous carbon is produced by impact/laser ablation, followed by CN radical production near the material boundary due to mixing between N_2 and C_2, and then hot CN radicals react further with the ambient atmosphere in the wake. Both vapors may follow a similar chemical evolution because they follow similar pressure–temperature paths.

In this study, the absolute CN yield in either experiments is given. The absolute CN yield, however, is not necessary for obtaining the HCN yield from aerodynamic ablation investigated in this study because CN is a transient product via chemical reactions under high temperature conditions. The HCN yield can be estimated from mass spectrometric measurements without knowing the amount of CN radicals. In this study, CN radicals were used as a tracer to assess the impact-and laser-induced chemical reaction fields because CN is the evidence of chemical interaction between the N-free direct vaporization products and the C-free ambient gas. The observed non-equilibrium nature of the vibrational state of CN radicals in both experiments indicates that the rate of CN formation by laser ablation is as fast as that by hypervelocity impacts in terms of the breakdown of vibrational equilibrium in emission spectra. Furthermore, the series of mass spectrometry using a variety of ambient gases as presented in Section 3.2.1 clearly show that the detected HCN in the laser experiments is resulted from such chemical reactions between direct vaporization products and the ambient gases. These experimental results support the validity of the laser experiments to investigate the conversion ratio from vaporized carbon to HCN because similar chemical reaction fields and reaction paths should lead to similar final products after the chemically quenching.

Scaling Effects of Vapor Clouds on Cyanide Production

The size of laser-generated ablation vapor clouds in the laboratory is much smaller than the impactor size colliding with the early Earth. Precise assessment for scaling effects would require extensive effort and beyond the scope of this study. Nevertheless, the size of hot vapor possibly affects the mixing efficiency between the ablation vapor and the ambient

atmosphere and the cooling rate, which controls quenching temperature. Thus, the potential scaling effects on cyanide production should be discussed. Sugita and Schultz (2009) pointed out that CN production processes after oblique impacts is controlled by the physical strength of impactor fragments and their impact velocity, and not by the size of impactor. Thus, the mixing efficiency between generated carbon vapor and the ambient atmosphere is not expected to decrease even at planetary scale impacts. An impact-comminuted projectile is further broken up by high aerodynamic ram pressure after oblique impacts (i.e., ~10^8 Pa at the translational velocity of 10 km/s mentioned in Section 4.1). The strength of stony meteorites and silicate melt droplets are 1–5×10^7 Pa (e.g., Hills and Goda 1993) and 3–5×10^6 Pa (Murase and McBirney 1973; Kadono et al. 2008), respectively, which are both much smaller than the ram pressure. Therefore, the size of each ablation vapor around impact fragments may approach that of laser-generated ablation vapors. Thus, laser ablation may produce similar chemical reaction field, including pressure, temperature, and chemical composition, as impact-induced aerodynamic interactions because laser-and impact-induced ablation vapors are likely to allow similar thermodynamic tracks.

Assessment for cooling time scale is more difficult. Based on spectroscopic observations, the temperature difference between CN and C_2 discussed in Section 3.1 indicate that fast thermal equilibration in a bulk vapor cloud does not occur. Thus, the cooling rate of the ablation vapor may be controlled by gas dynamics around each small fragment, including adiabatic expansion, radiation, and collision with cold ambient atmospheric gases, not impactor size. Then, the cooling rate will be fast; comparable to the cooling time scale of small laser plumes generated in the laboratory in this study. Then the conversion ratio from carbon to HCN obtained from the laser experiments in this study will be applicable rather directly. However, we could not rule out the possibility that individual small ablation vapor plumes coalesce into a large vapor plume and cool slowly at this stage. The situation would be more complicated. Thermodynamic calculations indicate that HCN yield does not depend on quenching temperature (i.e., cooling time scale) when the C/O ratio in a vapor plume is higher than unity (Chameides and Walker 1981). Then, HCN yield obtained in our laser experiments is applicable. If the C/O ratio is lower than unity, however, the HCN yield would decrease by a factor of about hundred as quenching temperature decreases (i.e., slower cooling) from 5,000 K to 1,500 K. Nevertheless, because the composition of ablation vapor is likely to stay reduced throughout its expansion and mixing with the ambient atmosphere as discussed above in the section 3.2.2, the dependence of HCN yield on scale would be rather weak. Thus, the carbon conversion ratio to HCN obtained in our laboratory experiments may serve as a good estimate for mid-size impact events on the early Earth.

Advantages of Impact-Induced Aerodynamic Ablation Compared in Cyanide Production

Chemical reactions during a dynamic event are very complicated. Understanding all the impact-driven processes at different time scales and location, however, is extremely difficult. Thus, we did not discuss exact chemical pathways from meteoritic carbon and atmospheric nitrogen to HCN in detail in this study. Nevertheless, we considered multiple candidate processes for HCN production associated with impact-induced vapor plume evolution within an atmosphere and assessed which physical process is the most efficient for HCN production in actual planetary-scale impacts based on chemical equilibrium. More specifically, three candidates for HCN production via impact-induced gas-phase chemical reactions are considered: (1) air heating within a bow shock induced by high-speed downrange-moving impactor fragments emerging from the impact point, (2) pure vaporization of projectile material, and (3) the aerodynamic ablation of impactor material investigated in this study. First and second processes, however, are

likely to be inefficient on the early Earth because of the following reasons. The HCN production efficiency by first process strongly depends on the redox state in an ambient atmosphere, not the physical consequence in air heating. Thus, the HCN yield by first process is expected to be low in the case of oblique impacts because the early Earth's atmosphere may be redox-neutral as discussed in the Section 1. The HCN production due to second process is limited by the nitrogen content in the impactor. In general, chondritic materials are highly depleted in nitrogen compared with biomolecules on the Earth as discussed in Section 1. Thus, first and second processes are essentially unfavorable for an efficient HCN production on the early Earth in terms of chemical composition. The HCN production efficiency is likely to be rather low independently of the size of vapor plumes. Therefore, third process, aerodynamic ablation around downrange-moving impactor fragments, is the most plausible process for investigating the HCN yield because the spectroscopically detected CN radicals clearly shows that the ablation vapor contains both C-rich impactor materials and an N-rich ambient atmosphere due to mixing. This process has a great advantage on HCN production because meteoritic material is highly depleted in nitrogen. Such an efficient mixing process does not occur in the case of nearly vertical impacts. Furthermore, the ablation vapor has a high temperature due to energy conversion from the kinetic energy of impactor to the internal energy of the ablation vapor, resulting in efficient dissociation of the triple bond of atmospheric nitrogen (N_2).

Impactors During the Heavy Bombardment Period

Another important consideration is the type of impactors, as carbon-rich impactors are required for efficient cyanide production. There are two populations of asteroids, which are the near Earth asteroids (NEA) and the main belt asteroids (MBA). Most of the recent meteorite falls to Earth are ordinary chondrites that come from NEA. The dominant type of NEA is S-type, which is considered to originate from the parent bodies of ordinary chondrites (Binzel et al. 2004). The size distribution of MBA is similar to the impactor size distribution during the heavy bombardment period (Strom et al. 2005), and the dominant type of MBA is C-type, which is considered to be the source of carbonaceous chondrites (Bus and Binzel 2002). Thus, carbonaceous chondrites are expected to have been the most frequent impactors during the heavy bombardment period, and hence the HCN generation mechanism investigated in this study may have been prominent during the heavy bombardment period.

The Column Density of Cyanides After Impacts on the Early Earth

We have shown above that the production efficiency of HCN obtained by laser ablation experiments is expected to be applicable to real impact processes. We now estimate the resulting column density of cyanides after oblique impacts by considering the macroscopic motion of impactors after oblique impacts, based on the conversion ratio obtained in Section 3.2.2 and a simple physical model. A downrange moving projectile with lateral dispersal motion is referred to as a "debris cloud". The equation of motion of debris clouds is given, for example, by Hills and Goda (1993):

$$m\,\dot{v} = -C_D\,\rho_a\,S\,v^2\,,$$
$$S = \pi\left(\frac{D_p}{2} + v_{disp}\Delta t\right)^2,$$
$$v_{disp} = \beta\; v_{impact}\;.$$

where m, v, C_D=0.5, ρ_a=1 kg/m^3, S, D_P=600 m, v_{disp}, Δt, β=0.5, and v_{impact}=17 km/s are the mass of the debris cloud, translational velocity, drag coefficient, cross section of the debris

cloud, density of the ambient atmosphere, projectile diameter, lateral dispersal velocity of the debris cloud, time after the impact, a coefficient estimated by the impact experiments, and typical impact velocity (e.g., Ito and Malhotra 2006), respectively. We neglected deceleration of the dispersion velocity and the atmospheric structure for these first-order calculations. The deposition area is estimated to be ~10^2 km^2. The carbon content of a carbonaceous body (CI-like) 600 m in diameter is ~8×10^{11} mol (Wasson and Kallemeyn 1988). Using a conversion ratio of 0.1 mol% for converting vaporized carbon to HCN, the column density of HCN after impacts is ~10 mol/m^2 over ~10^2 km^2 of surface area. This column density is equivalent to 500–10,000 years of accumulated HCN production by lightning within a strongly reducing (i.e., highly fertile) atmosphere (e.g., Stribring and Miller 1986). Cyanides condensates are also produced over this area.

If all produced HCN injected on a lake or shallow marsh 1 m in depth via rain out, resulting HCN concentration reaches a possible range for adenine synthesis, 0.01 mol/L [e.g., Chang et al. 1983; Ferris and Hagan 1984; Miyakawa et al. 2002a, b]. Actual chemical conversion rate from simple cyanide compounds, such as HCN, to more complex biologically important more complex molecules, such as adenine, depends on many factors, such as temperature and pH of water (e.g., Miyakawa et al. 2002a). Nevertheless, a large surface area (~10^2 km^2) covered by fallout from a mid-size impactor, may contain a variety of surface conditions. Furthermore, the relatively small projectile size considered in this study would hit the Earth extremely frequently; a projectile 1 km in diameter or larger every ~1 month during the heavy bombardment period (e.g., Bottke et al. 2010). Then a very large surface area on Earth would have received a high-column density of cyanide many times. Then, if a temperature and pH conditions suitable for subsequent chemical evolution occurred near the surface, such sites are very likely to have received thick CN-loaded deposit. Because of the high concentration of cyanide, such localities may have led to high abundance of adenine and/or perhaps amino acid.

Note that impactors with <300 m in diameter are burned out during atmospheric passage under the current Earth's atmospheric condition [e.g., Melosh 1989]. The HCN production due to aerodynamic ablation around small high-speed fragments investigated in this study, however, would occur in a very similar way as discussed in Sections 4.1 and 4.2 even when the impactor is burned out in the atmosphere. This is because the "burn out" of such small impactors are estimated to be caused by mechanical disruption by aerodynamic ram pressure [e.g., Melosh 1989; Schultz 1992; Hills and Goda 1993; Artemieva and Shuvalov 2001]. Then, a cloud of high-speed fragments will form and aerodynamic ablation will occur, which will lead to intense chemical reaction between impactor-derived material and atmospheric gas.

Conclusions

We have conducted hypervelocity impact and laser ablation experiments within simulated early Earth's atmospheres to investigate cyanide production processes due to mid-size impactors (0.1–1 km in diameter). In situ spectroscopic observation of hypervelocity oblique impacts provides information on the thermodynamic state of the impact-induced ablation vapor. We obtained two qualitative similarities (i.e., spectral outline and vibrational non-equilibrium), and a quantitative agreement (i.e., translational-rotational temperature), between impact-and laser-induced ablation vapors, demonstrating that laser ablation can simulate CN production processes due to aerodynamic ablation after oblique impacts, including vibrational non-equilibrium. A series of laser ablation experiments showed that a part of the destroyed organic matter in the projectile is converted into cyanide compounds via subsequent chemical

reactions with the ambient gases, even though the ambient gases contains as much as ~400 mbar CO_2. We found that the conversion ratio of vaporized carbon to gaseous HCN is 0.1–2 mol% under partial pressures of CO_2 from 0 mbar to 390 mbar. The condensed-phase analyses show that nitrogen in an ambient atmosphere is incorporated into the condensed products by forming C≡N, −N=C=N, and C=N bonds. These experimental results suggest that the aerodynamic ablation of carbon-containing impactors in a N_2-rich atmosphere could have ultimately produced complex organic molecules containing cyanides on the early Earth. A simple model for the fragment dispersal dynamics of impacted bodies shows that the resulting column density is equivalent to ~1×10^4 year of HCN production by lightning in a strongly reducing atmosphere. Such a concentrated supply of cyanides due to small impacts may have played an important role in the origin of life on Earth.

Acknowledgments Hypervelocity impact experiments performed in this study were supported by the Institute of Space and Astronautical Science of the Japan Aerospace Exploration Agency, as a collaborative program of the Space Plasma Experiment. The authors appreciate M. Tabata for his help in the hypervelocity impact experiment. The authors thank R. Ishimaru, T. Sasaki, K. Fujita, K. Suzuki, M. Okada, and Y. Takase for their insightful comments. The authors also thank an anonymous referee for his critical reviews which helped improve the manuscript greatly and A. Schwartz for helpful comments as an editor. K. K. also thanks the members of the Graduate School of Environmental Studies of Nagoya University, S. Watanabe, M. Furumoto, and Y. Shimaki, for their support during writing of this manuscript. This study was supported in part by a Grant-in-Aid from the Japan Society for the Promotion Science.

References

Artemieva NA, Shuvalov VV (2001) Motion of a fragmented meteoroid through the planetary atmosphere. J Geophys Res 106:3297–3309

Binzel RP, Rivkin AS, Stuart JS et al (2004) Observed spectral properties of near-earth objects: Results for population distribution, source regions, and space weathering processes. Icarus 170:259–294

Blank JG, Miller GH, Ahrens MJ, Winans RE (2001) Experimental shock chemistry of aqueous amino acid solutions and the cometary delivery of prebiotic compounds. Orig Life Evol Biosph 31:15–51. doi:10.1023/A:1006758803255

Bottke WF, Walker RJ, Day JMD et al (2010) Stochastic late accretion to earth, the moon, and mars. Science 330:1527–1530

Bus SJ, Binzel RP (2002) Phase II of the small main-belt asteroid spectroscopic survey a feature-based taxonomy. Icarus 158:146–177

BVSP (1981) Basaltic volcanism on the terrestrial planets. Pergamon, New York

Canup RM (2004) Simulations of a late lunar-forming impact. Icarus 168:433–456

Chameides WL, Walker JCG (1981) Rates of fixation by lightning of carbon and nitrogen in possible primitive atmosphere. Orig Life Evol Biosph 11:291–302

Chang S, Des Marais D, Mack R et al. (1983) Prebiotic organic synthesis and the origin of life. In Schopf JW (ed) Earth's Earliest Biosphere: Its Origin and Evolution. Princeton University Press, pp 53–92

Chapin FS, Matson PA III, Mooney HA (2008) Principles of terrestrial ecosystem ecology. Springer, New York

Chyba CF (1991) Terrestrial mantle siderophiles and the lunar impact record. Icarus 92:217–233

Chyba CF, Sagan C (1992) Endogeneous production, exogeneous delivery and impact-shock synthesis of organic molecules: An inventory for the origins of life. Nature 355:125–132

Cooper G, Kimmich N, Belisle W et al (2001) Carbonaceous meteorites as a source of sugar-related organic compounds for the early Earth. Nature 414:879–883

Cronin JR, Pizzarello S, Cruikshank DP (1988) Organic matter in carbonaceous chondrites, planetary satellites, asteroids and comets. In Meteorites and the Early Solar System. University of Arizona Press, pp 819–857

Fegley B, Prinn RG, Hartman H, Watkins H (1986) Chemical effects of large impacts on the Earth's primitive atmosphere. Nature 319:305–308

Ferris JP, Hagan WJ (1984) HCN and chemical evolution: The possible role of cyano compounds in prebiotic synthesis. Tetrahedron 40:1093–1120

Fujita K (2007) Assessment of molecular internal relaxation and dissociation by DSMC-QCT analysis. 39th AIAA Thermophysics Conference, Miami
Fujita K, Abe T (1997) SPRADIAN, structured package for radiation analysis: Theory and application. ISAS report 669:1–47
Gerasimov MV, Ivanov BA, Yakovlev OI, Dikov YP (1998) Physics and chemistry of impacts. Earth Moon Planet 80:209–259. doi:10.1023/A:1006322032494
Hashimoto GL, Abe Y, Sugita S (2007) The chemical composition of the early terrestrial atmosphere: Formation of a reducing atmosphere from CI-like material. J Geophys Res 112, E05010. doi:10.1029/2006JE002844
Hayatsu R, Anders E (1981) Organic compounds in meteorites and their origins. Top Curr Chem 99:1c–37
Hertzberg G (1950) Molecular spectra and molecular structure, I, diatomic molecules, 2nd edn. Van Nostrand, Princeton
Hills JG, Goda MP (1993) The fragmentation of small asteroids in the atmosphere. Astron J 105:1114–1144
Hirschmann MM (2012) Magma ocean influence on early atmosphere mass and composition. Earth and Planetary Sci Lett 341–344:48–57
Imanaka H, Khare BN, Elsila JE, Bakes ELO, McKay CP, Cruikshank DP, Sugita S, Matsui T, Zare RN (2004) Laboratory experiments of Titan tholin formed in cold plasma at various pressures: implications for nitrogen-containing polycyclic aromatic compounds in Titan haze. Icarus 168:344–366
Ishibashi K, Ohno S, Sugita S et al (2006) Oxidation carbon compounds by SiO_2-derived oxygen within laser-induced vapor clouds. Lunar Planet Sci Conf XXXVII:1721
Ishibashi K, Ohno S, Sugita S et al. (2013) Oxidation carbon compounds by silica-derived oxygen within impact-induced vapor clouds. *Earth, Planet, Space*, in press
Ito T, Malhotra R (2006) Dynamical transport of asteroid fragments from υ6 resonance. Adv Space Res 38:817–825
Kadono T, Sugita S, Mitani NK et al. (2002) Vapor clouds generated by laser ablation and hypervelocity impact. Geophys Res Lett 29. doi: 10.1029/2002GL015694
Kadono T, Arakawa M, Kouchi A (2008) Size distributions of chondrules and dispersed droplets caused by liquid breakup: an application to shock wave conditions in the solar nebula. Icarus 197:621–626
Kasting JF (1990) Bolide impacts and the oxidation state of carbon in the Earth's early atmosphere. Orig Life Evol Biosph 20:199–231
Kasting JF (1993) Earth's Early atmosphere. Science 259:920–926
Kulikov YN, Lammer H, Lichtenegger HIM et al (2007) A comparative study of the atmospheres of earth, venus, and mars. Space Sci Rev 129:207–243
Kurosawa K, Sugita S, Fujita K et al (2009) Rotational-temperature measurements of chemically reacting CN using band-tail spectra. J Thermophys Heat Transfer 23:463–472
Kurosawa K, Ohno S, Sugita S et al (2012) The nature of shock-induced calcite ($CaCO_3$) devolatilization in an open system investigated using a two-stage light gas gun. Earth Planet Sci Lett 337–339:68–76
McKay CP, Borucki WJ (1997) Organic synthesis in experimental impact shocks. Science 276:390–392
Melosh HJ (1989) Impact cratering: A geologic process. 210 pp. Oxford University Press
Miller SL (1953) A production of amino acids under possible primitive Earth conditions. Science 117:528–529
Miller SL, Schlesinger G (1983) The atmosphere of the primitive Earth and the prebiotic synthesis of organic compounds. Adv Space Res 3:47–53
Miyakawa S, Cleaves FJ, Miller SL (2002a) The cold origin of life: A. Implications based on the hydrolytic stabilities of hydrogen cyanide and formamide. Orig Life Evol Biosph 32:195–208
Miyakawa S, Cleaves FJ, Miller SL (2002b) The cold origin of life: B. Implications based on pyrimidines and purines produced from frozen ammonium cyanide solutions. Orig Life Evol Biosph 32:209–218
Mukhin LM, Gerasimov MV, Safonova EN (1989) Origin of precursors of organic molecules during evaporation of meteorites and mafic terrestrial rocks. Nature 340:46–49
Murase T, McBirney AR (1973) Properties of some common igneous rocks and their melts at high temperatures. Geol Soc Am Bull 84:3563–3592
Ohkouchi N, Nakajima Y, Okada H et al (2005) Biogeochemical processes in a meromictic Lake Kaiike: Implications from carbon and nitrogen isotopic compositions of photosynthetic pigments. Environ Microbiol 7:1009–1016
Ohno S, Sugita S, Kadono T et al (2004) Sulfur chemistry in laser-simulated impact vapor clouds: Implications for the K/T impact event. Earth Planet Sci Lett 218:347–361
Pierazzo E, Melosh HJ (2000) Hydrocode modeling of oblique impacts: The fate of the projectile. Meteor Planet Sci 35:117–130
Pizzarello S (2012) Hydrogen cyanide in the Murchison meteorite, *The Astrophysical Journal Letters*, **754**, doi:10.1088/2041-8205/754/2/L27
Rao CNR (1963) Chemical applications of infrared spectroscopy. Academic, New York

Rosing MT (1999) C-13-depleted carbon microparticles in >3700-Ma sea-floor sedimentary rocks from west Greenland. Science 283:674–676
Ryder G (1990) Lunar samples, lunar accretion and the early bombardment of the Moon. EOS Trans AGU 71:322–395
Sagan C, Chyba C (1997) The early faint sun paradox: Organic shielding of ultraviolet-labile greenhouse gases. Science 276:1217–1221
Schaefer L, Fegley B Jr (2010) Chemistry of atmospheres formed during accretion of the Earth and other terrestrial planets. Icarus 208:438–448
Schidlowski M (1988) A 3,800-million-year isotopic record of life from carbon in sedimentary rocks. Nature 333:313–318
Schultz PH (1992) Atmospheric effects on ejecta emplacement and crater formation on Venus from Magellan. J Geophys Res 97:16183–16248
Schultz PH, Gault DE (1990) Prolonged global catastrophes from oblique impacts. Geol Soc Am Special Paper 247:239–261
Schultz PH, Sugita S (1996) Fate of the Chicxulub impactor (abstract). Lunar Planet Sci Conf 28:1261–1262
Sekine Y, Sugita S, Kadono T, Matsui T (2003) Methane production by large iron meteorite impacts on early Earth. J Geophys Res 108(E7):5070. doi:10.1029/2002JE002034
Sharma AK, Thareja RK (2005) Plume dynamics of laser-produced aluminum plasma in ambient nitrogen. Appl Surf Sci 243:68–75
Slack MW (1976) Kinetics and thermodynamics of the CN molecule. III. Shock tube measurement of CN dissociation dates. J Chem Phys 64:228–236
Stribring R, Miller SL (1986) Energy yields for hydrogen cyanide and formaldehyde syntheses: The HCN and amino acid concentrations in the primitive ocean. Orig Life Evol Biosph 17:261–273
Strom RG, Manuhotra R, Ito T, Yoshida F, Kring DA (2005) The origin of planetary impactors in the inner solar system. Science 309:1847–1850
Sugita S, Schultz PH (2003a) Interactions between impact-induced vapor clouds and the ambient atmosphere: 1. Spectroscopic observations using diatomic molecular emission. J Geophys Res 108(E6):5051. doi:10.1029/2002JE001959
Sugita S, Schultz PH (2003b) Interactions between impact-induced vapor clouds and the ambient atmosphere: 2. Theoretical modeling. J Geophys Res 108(E6):5052. doi:10.1029/2002JE001960
Sugita S, Schultz PH (2009) Efficient cyanide formation due to impacts of carbonaceous bodies on a planet with a nitrogen-rich atmosphere. Geophys Res Lett 36, L20204. doi:10.1029/2009GL040252
Tera F, Papanastassiou DA, Wasserburg GJ (1974) Isotopic evidence for a terminal lunar cataclysm. Earth Planet Sci Lett 22:1–21
Thareja RK, Dwivedi RK, Ebihara K (2002) Interactions of ambient nitrogen gas and laser ablated carbon plume: Formation of CN. Nucl Instrum Meth Phys Res B 192:301–310
Trail D, Watson EB, Tailby ND (2011) The oxidation state of Hadean magmas and implications for early Earth's atmosphere. Nature 480:79–82
Vivien C, Hermann J, Perrone A et al (1998) A study of molecule formation during laser ablation of graphite in low-pressure nitrogen. J Phys D: Appl Phys 31:1263–1272
Wasson JT, Kallemeyn WK (1988) Composition of chondrites. Phil Trans R Soc Lond A 325:535–544
Wee S, Park SM (1999) Reactive laser ablation of graphite in a nitrogen atmosphere: Optical emission studies. Opt Comm 165:199–205
Zahnle KJ (1986) Photochemistry of methane and the formation of hydrocyanic acid (HCN) in the Earth's early atmosphere. J Geophys Res 91:2819–2834
Zahnle KJ, Schaefer L, Fegley B Jr (2011) Earth's earliest atmosphere. CSH Persp Biol 2:a004895. doi:10.1101/cshperspect.a004895